Supplementary Figures

for "Pressure-, temperature- and water-dependent melting in silica-rich rocks — new parametrization and its application in models of porous melt flow" by

P. Maierová[1], P. Štípská[1], P. Hasalová[1], K. Schulmann[1], R. Weinberg[2], O. Souček[3]

[1] Czech Geological Survey, Klárov 3/131, 118 00, Prague 1, Czech Republic.
[2] School of Earth Atmosphere and Environment, Monash University, Clayton, Victoria 3800, Australia
[3] Mathematical Institute, Faculty of Mathematics and Physics, Charles University, Sokolovská 83, Prague 8, Czech Republic.

Corresponding author: P. Maierová
Email: petra.maierova@geology.cz

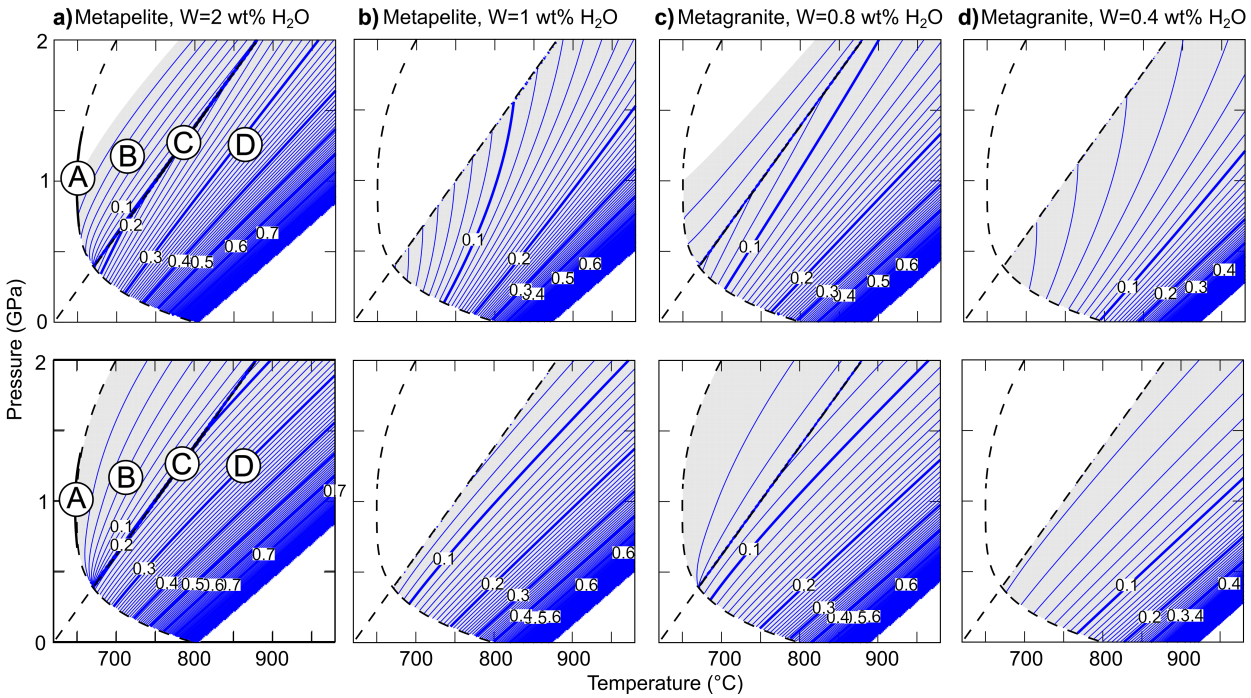

Figure S1: Melt fractions from parametrization with and without pressure dependence of $w_{1,2,3}$. Upper row of panels: melt fraction calculated from the parametrization including the pressure dependence of $w_{1,2,3}$. Parameters for "metapelite": $w_{01} = 0.5$, $w_{02} = 1.5$, $w_{03} = 2.0$, $w_{P1} = -0.5$, $w_{P2} = 0.0$, $w_{P3} = 0.4$; for "metagranite": $w_{01} = 0.2$, $w_{02} = 0.6$, $w_{03} = 0.8$, $w_{P1} = -0.2$, $w_{P2} = 0.0$, $w_{P3} = 0.4$; all in wt% H_2O. Lower row of panels: melt fraction calculated from the parametrization neglecting the pressure dependence of $w_{1,2,3}$. Parameters are the same as for the upper row, except for $w_{P1,2,3} = 0$. Blue contours show melt fraction. Black dashed lines show parameterized wet solidus (A) and muscovite terminal breakdown (C). B and D are regions where gradual melting reactions take place.

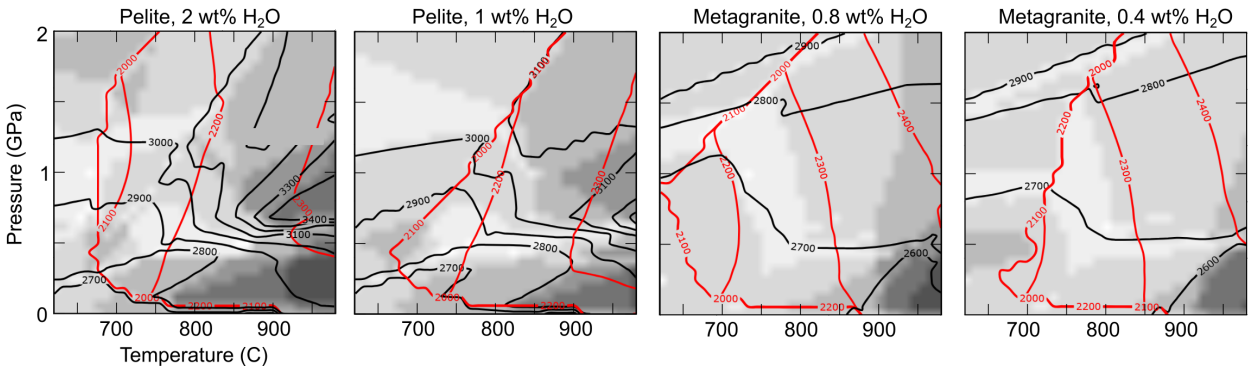

Figure S2: Phase-equilibria modeling results computed using MAGEMin software Riel et al. (2022), with the thermodynamic dataset by White et al. (2014) for metapelite, and the updated dataset by Green et al. (2025), previously Holland et al. (2018), for metagranite. The four panels correspond to the lower row of panels in Fig. 2 in the main text and were computed with the same method and parameters. Black and red lines are contours of the density of the solid and melt phase, respectively. Labels are in $\mathrm{kg\,m^{-3}}$. The grey fields in the background show the stability of individual mineral assemblages, separated by boundaries where one mineral appears or disappears.

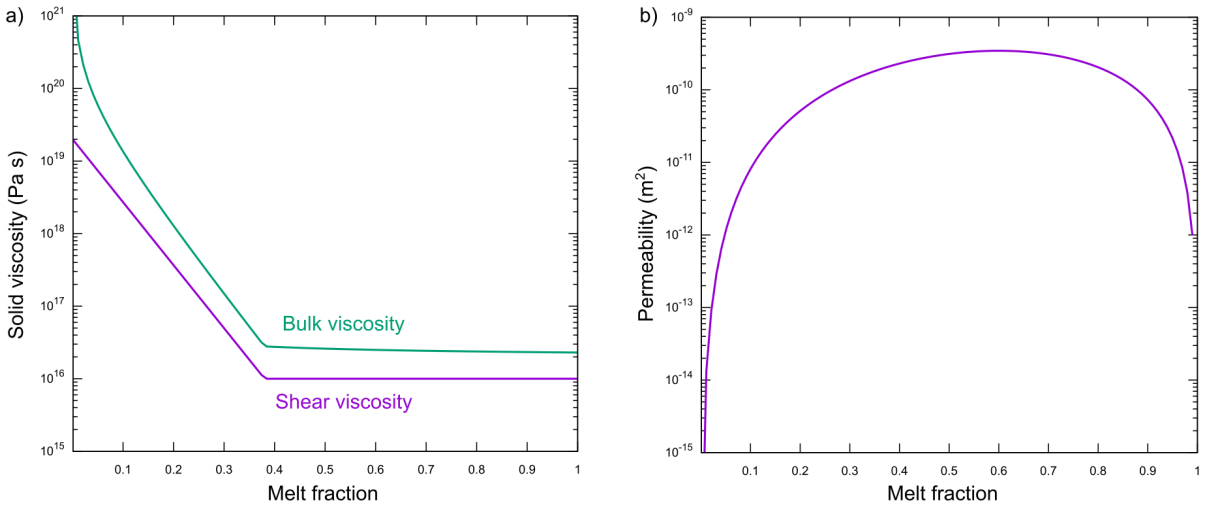

Figure S3: The shear and bulk viscosity of the solid at $T = 800\,^{\circ}\mathrm{C}$ (panel a) and the permeability (panel b) as they depend on the melt fraction according to equations (8), (9) and (11) in the main text.

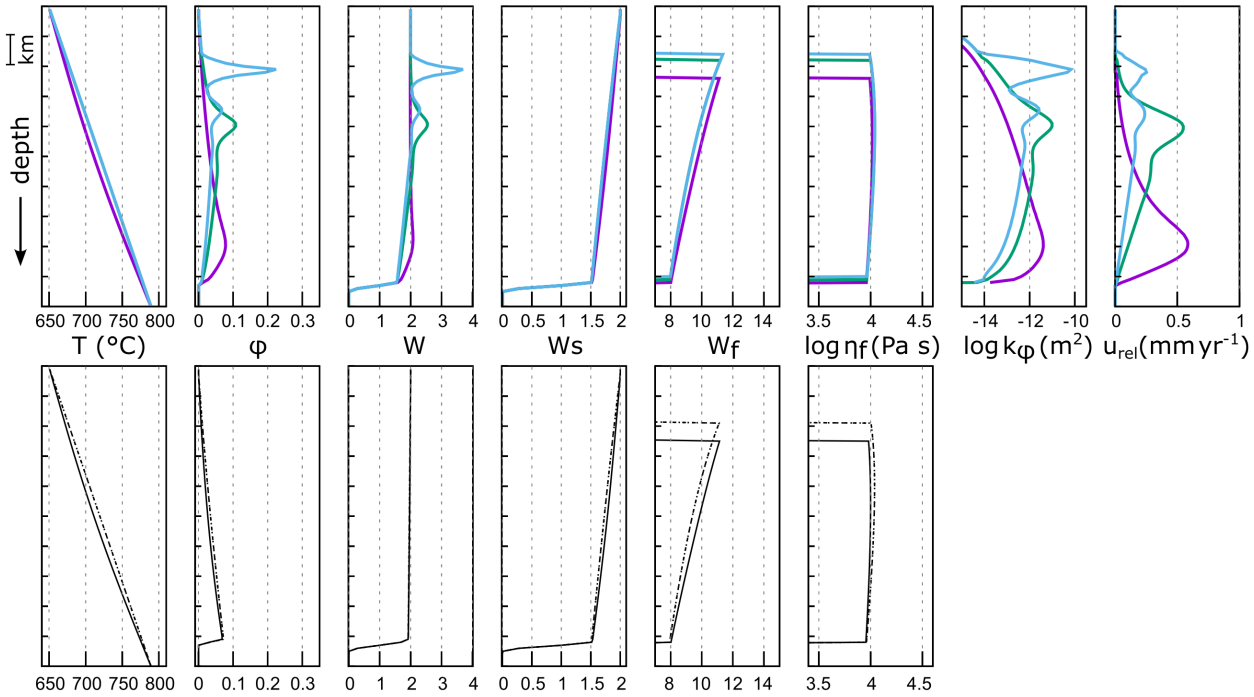

Figure S4: Results of the two-phase flow model (upper row of panels) and of the case where the melt percolation through the solid is switched off (lower row). Model parameters are: $P_{\text{top}} = 1\,\text{GPa}$, $T_{\text{top}} = 650\,^{\circ}\text{C}$, $T_{\text{bot}} = 790\,^{\circ}\text{C}$. Parameters in the melting law for "metapelite"; $W_0 = 2$. Individual panels show variations of model properties (temperature T, melt fraction ϕ, bulk water content W, solid water content W_s, melt water content W_f, melt viscosity η_f, permeability k_ϕ and relative velocity between the melt and the solid $u_{\text{rel}} = u_f - u_s$) with depth at three different time steps. Purple, green and blue lines show the results at 1, 5 and 10 Myr of model evolution accounting for the melt percolation through the solid (two-phase flow). Solid, dashed and dotted black lines show the results at 1, 5 and 10 Myr if melt percolation is switched off (for T, W_s, W_f and η_f, the result is visually the same as with melt percolation; k_ϕ and u_{rel} are zero by definition).

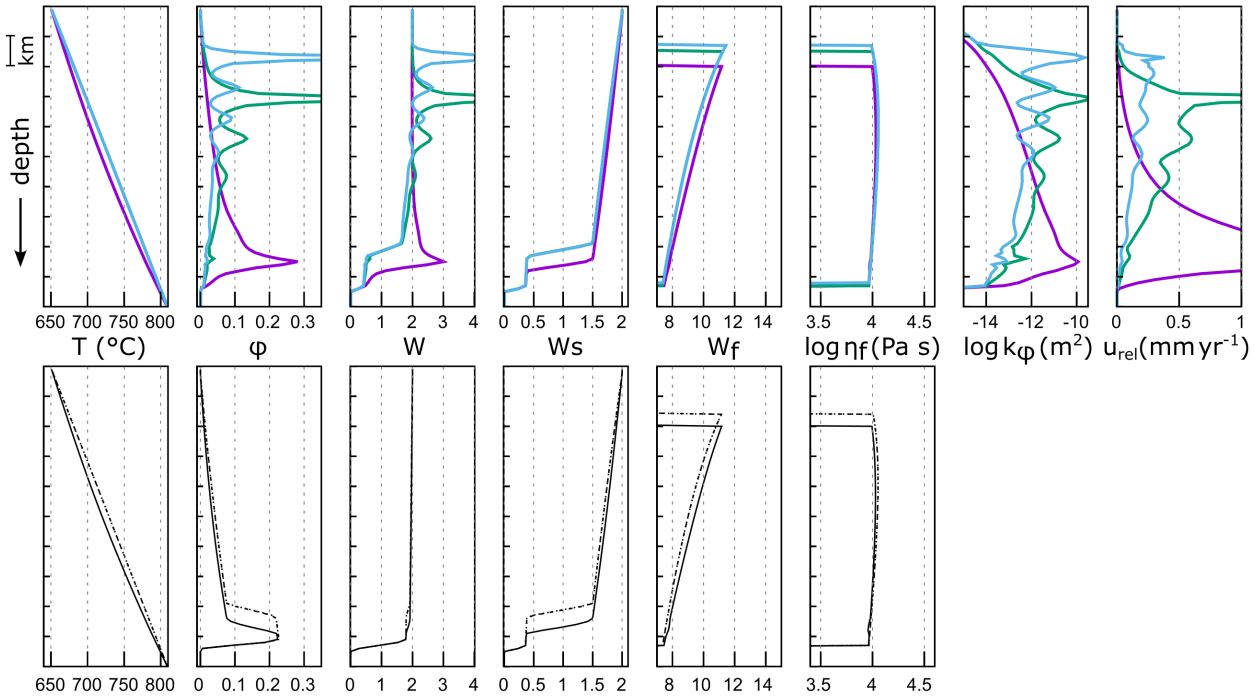

Figure S5: Model parameters are: $P_{\text{top}} = 1\,\text{GPa}$, $T_{\text{top}} = 650\,^{\circ}\text{C}$, $T_{\text{bot}} = 810\,^{\circ}\text{C}$. Parameters in the melting law for "metapelite"; $W_0 = 2.0$. Figure layout is the same as in Figure S4.

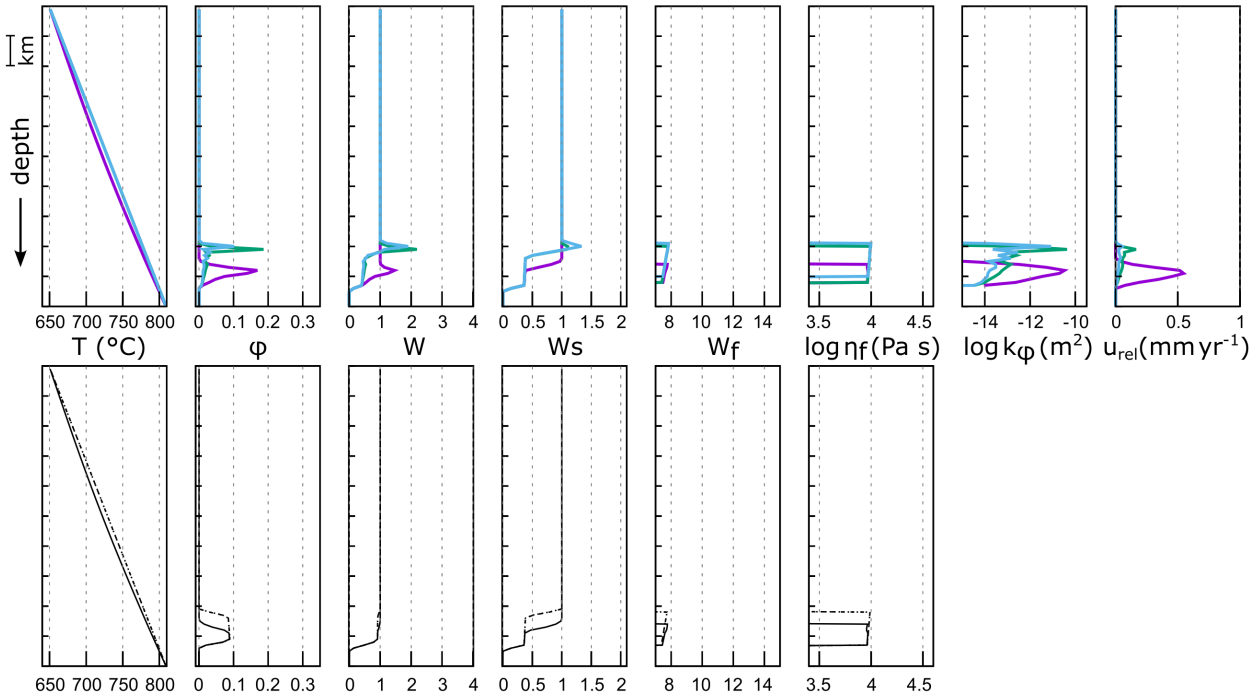

Figure S6: Model parameters are: $P_{\text{top}} = 1\,\text{GPa}$, $T_{\text{top}} = 650\,^{\circ}\text{C}$, $T_{\text{bot}} = 810\,^{\circ}\text{C}$. Parameters in the melting law for "metapelite"; $W_0 = 1.0$. Figure layout is the same as in Figure S4.

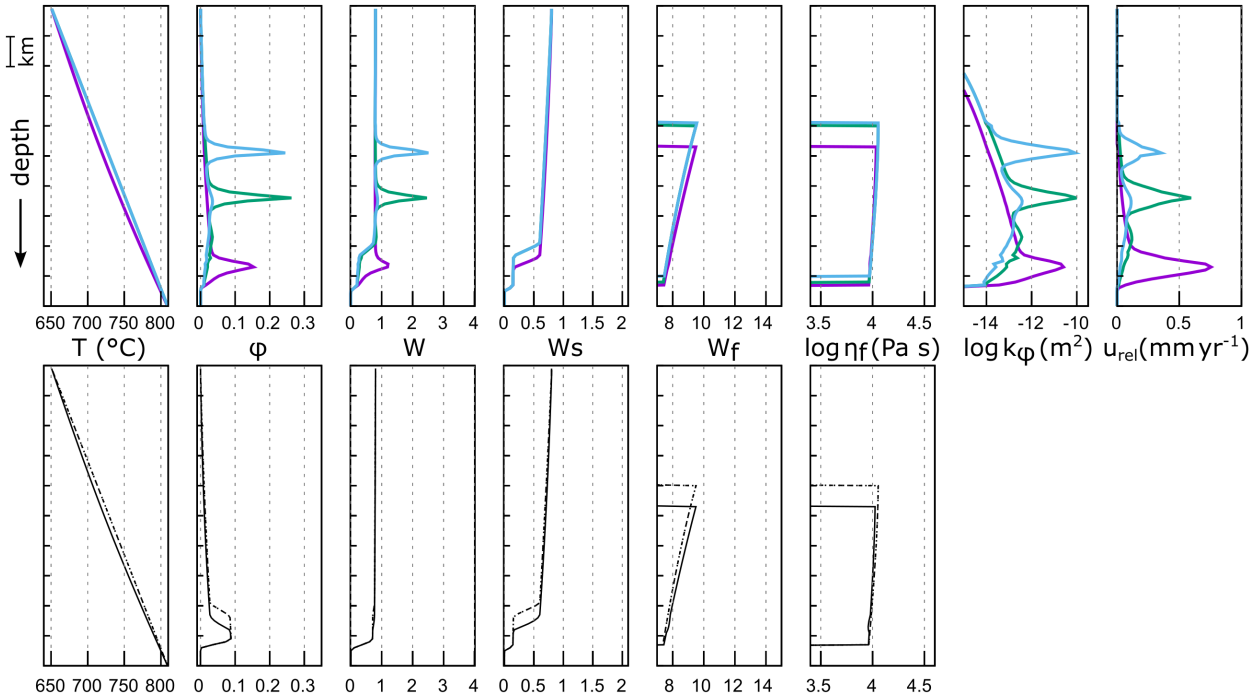

Figure S7: Model parameters are: $P_{\text{top}} = 1\,\text{GPa}$, $T_{\text{top}} = 650\,^{\circ}\text{C}$, $T_{\text{bot}} = 810\,^{\circ}\text{C}$. Parameters in the melting law for "metagranite"; $W_0 = 0.8$. Figure layout is the same as in Figure S4.

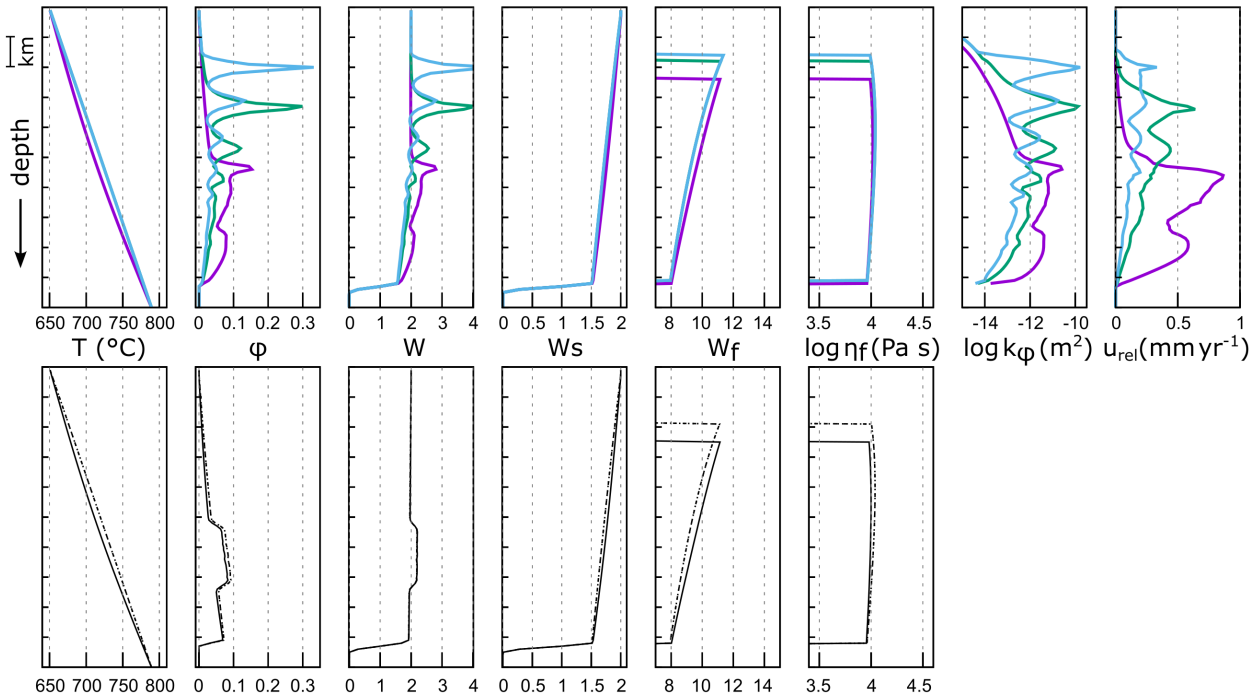

Figure S8: Model parameters are: $P_{\text{top}} = 1\,\text{GPa}$, $T_{\text{top}} = 650\,^{\circ}\text{C}$, $T_{\text{bot}} = 790\,^{\circ}\text{C}$. Parameters in the melting law for "metapelite". $W_0 = 2.0$ except for a middle layer with an increased initial water content, $W_{0,\text{anom}} = 2.3$. Figure layout is the same as in Figure S4.

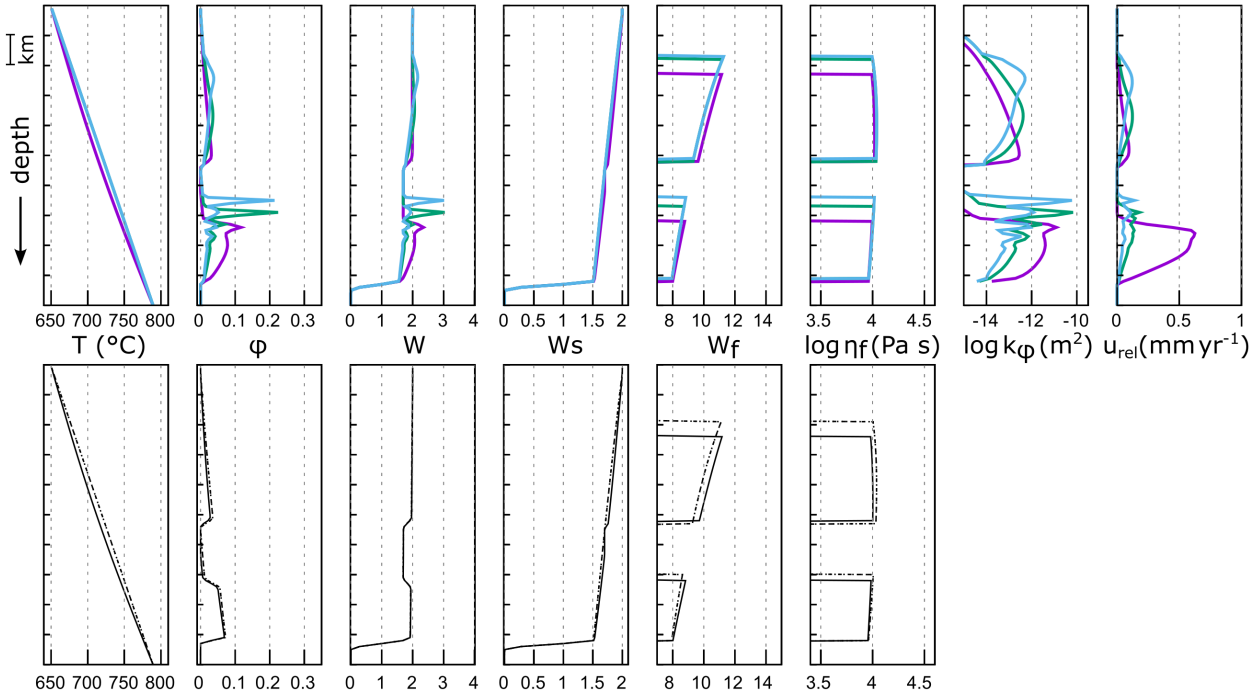

Figure S9: Model parameters are: $P_{\text{top}} = 1\,\text{GPa}$, $T_{\text{top}} = 650\,^{\circ}\text{C}$, $T_{\text{bot}} = 790\,^{\circ}\text{C}$. Parameters in the melting law for "metapelite". $W_0 = 2.0$ except for a middle layer with a decreased initial water content, $W_{0,\text{anom}} = 1.7$. Figure layout is the same as in Figure S4.

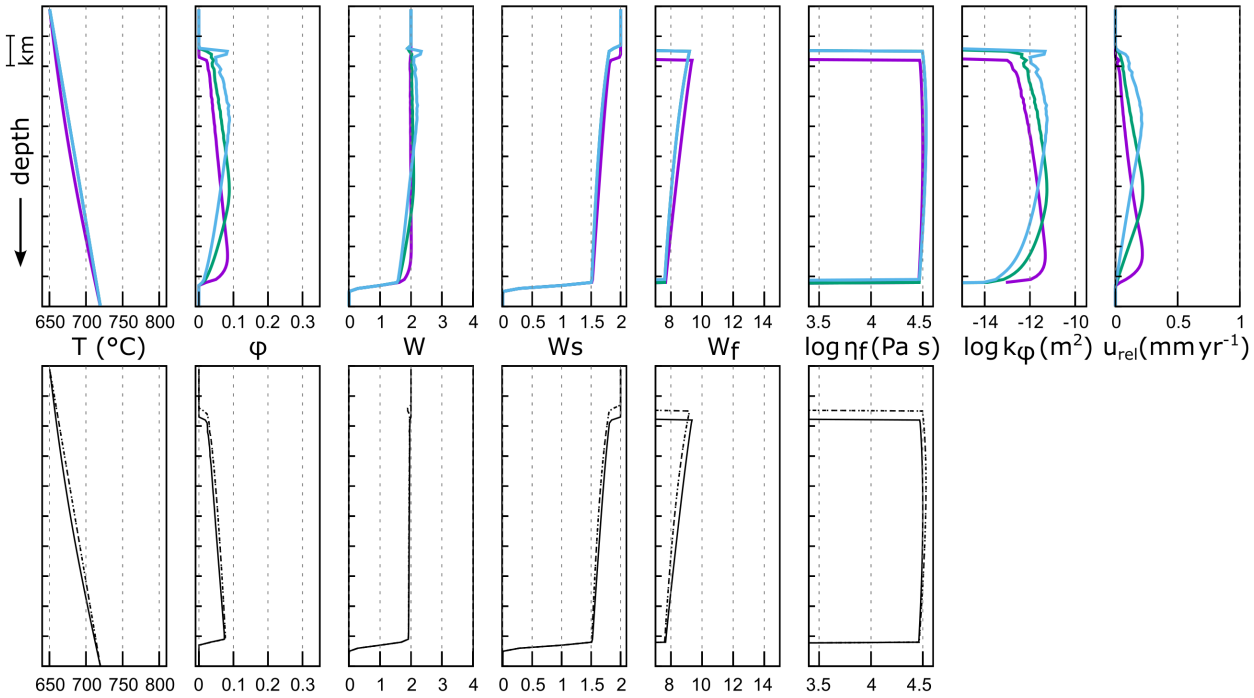

Figure S10: Model parameters are: $P_{\text{top}} = 0.5\,\text{GPa}$, $T_{\text{top}} = 650\,^{\circ}\text{C}$, $T_{\text{bot}} = 720\,^{\circ}\text{C}$. Parameters in the melting law are for "metapelite"; $W_0 = 2$. Figure layout is the same as in Figure S4.

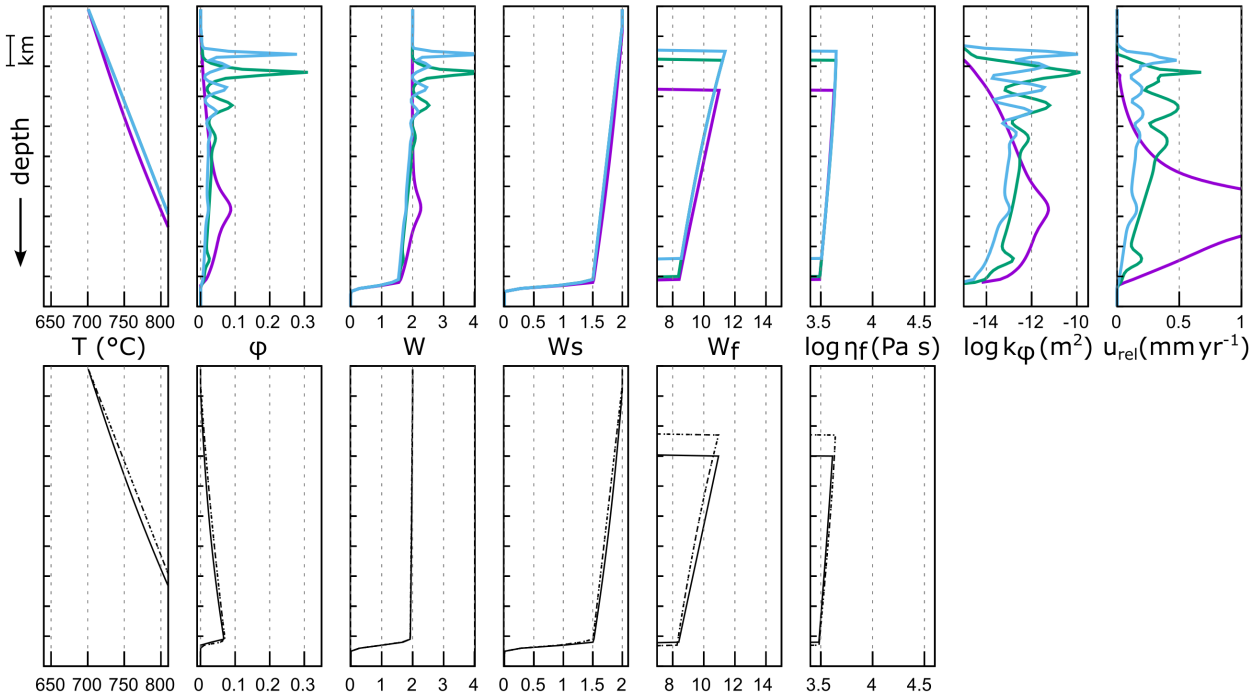

Figure S11: Model parameters are: $P_{\text{top}} = 1.5\,\text{GPa}$, $T_{\text{top}} = 700\,^{\circ}\text{C}$, $T_{\text{bot}} = 860\,^{\circ}\text{C}$. Parameters in the melting law for "metapelite"; $W_0 = 2$. Figure layout is the same as in Figure S4.

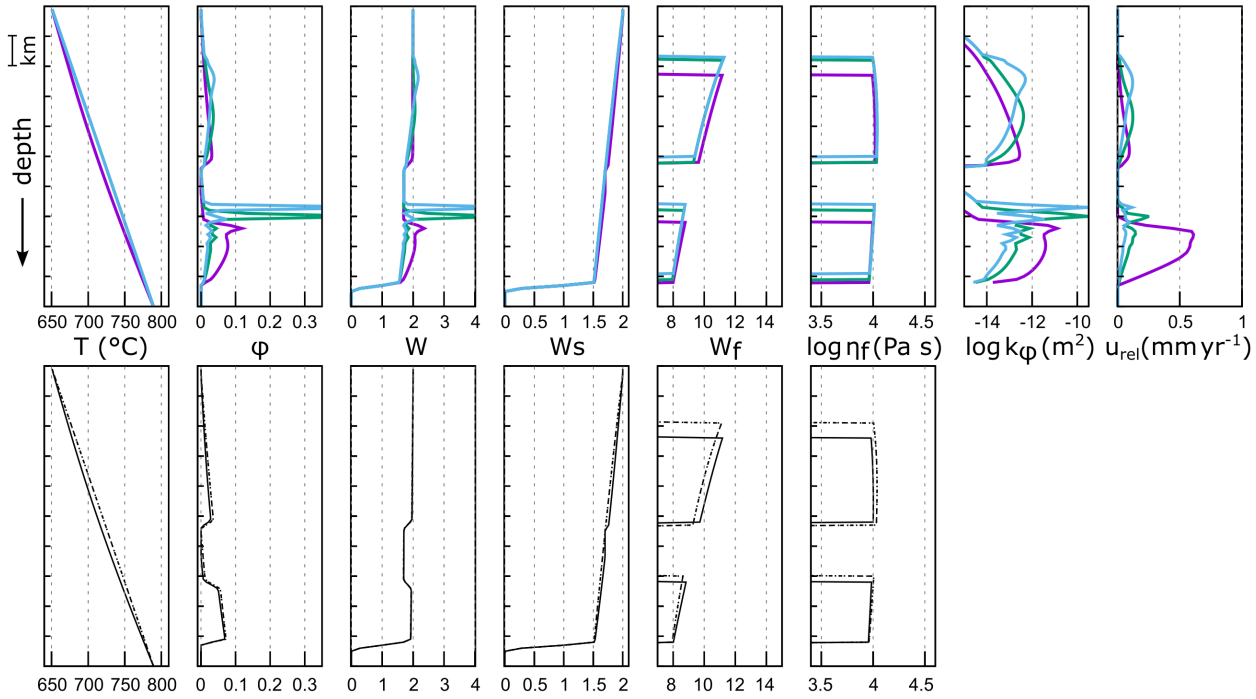

Figure S12: Model parameters are the same as for Fig. S9, except for a higher resolution with 400 elements in the vertical direction. ($P_{\mathrm{top}} = 1\,\mathrm{GPa}$, $T_{\mathrm{top}} = 650\,^{\circ}\mathrm{C}$, $T_{\mathrm{bot}} = 790\,^{\circ}\mathrm{C}$, "metapelite" melting law, $W_0 = 2.0$ except for a middle layer with $W_{0,\mathrm{anom}} = 1.7$.) The high resolution causes finer focusing of melt beneath the low-porosity layer, which presents a low-permeability obstacle for the flow. Figure layout is the same as in Figure S4.

References

Green, E. C. R., Holland, T. J. B., Powell, R., Weller, O. M., and Riel, N.: Corrigendum to: Melting of Peridotites through to Granites: a Simple Thermodynamic Model in the System KNCFMASHTOCr, and, a Thermodynamic Model for the Subsolidus Evolution and Melting of Peridotite. | Journal of Petrology | Oxford Academic, 66, https://doi.org/https://doi.org/10.1093/petrology/egae079, 2025.

Holland, T. J. B., Green, E. C. R., and Powell, R.: Melting of Peridotites through to Granites: A Simple Thermodynamic Model in the System KNCFMASHTOCr, Journal of Petrology, 59, 881–900, https://doi.org/10.1093/petrology/egy048, 2018.

Riel, N., Kaus, B. J. P., Green, E. C. R., and Berlie, N.: MAGEMin, an Efficient Gibbs Energy Minimizer: Application to Igneous Systems, Geochemistry, Geophysics, Geosystems, 23, e2022GC010 427, https://doi.org/10.1029/2022GC010427, 2022.

White, R. W., Powell, R., Holland, T. J. B., Johnson, T. E., and Green, E. C. R.: New mineral activity–composition relations for thermodynamic calculations in metapelitic systems, Journal of Metamorphic Geology, 32, 261–286, https://doi.org/10.1111/jmg.12071, 2014.